

## Prediction of ambient pressure superconductivity in cubic ternary hydrides with $MH_6$ octahedra

Feng Zheng<sup>a,b,1</sup>, Zhen Zhang<sup>c,1</sup>, Zepeng Wu<sup>b</sup>, Shunqing Wu<sup>b,\*\*</sup>, Qiubao Lin<sup>a</sup>, Renhai Wang<sup>d</sup>, Yimei Fang<sup>b</sup>, Cai-Zhuang Wang<sup>c,e</sup>, Vladimir Antropov<sup>c,e</sup>, Yang Sun<sup>b,\*</sup>, Kai-Ming Ho<sup>c</sup>

<sup>a</sup> School of Science, Jimei University, Xiamen, 361021, China

<sup>b</sup> Department of Physics, Xiamen University, Xiamen, 361005, China

<sup>c</sup> Department of Physics and Astronomy, Iowa State University, Ames, IA, 50011, USA

<sup>d</sup> School of Physics and Optoelectronic Engineering, Guangdong University of Technology, Guangzhou, 510006, China

<sup>e</sup> Ames National Laboratory, U.S. Department of Energy, Ames, IA, 50011, USA

### ABSTRACT

Exploring high-temperature superconducting (high- $T_c$ ) material at ambient pressure holds immense significance for physics, chemistry, and materials science. In this study, we perform a high-throughput screening of strong electron-phonon interactions in  $X_2MH_6$  compounds ( $X = Li, Na, Mg, Al, K, Ca, Ga, Rb, Sr$ , and  $In$ ;  $M$  are  $3d$ ,  $4d$ , and  $5d$  transition metals). These compounds have a cubic structure featuring an  $MH_6$  octahedron motif. Our screening calculations suggest that 26 compounds exhibit dynamic stability and strong electron-phonon coupling. Among them,  $Mg_2RhH_6$ ,  $Mg_2IrH_6$ ,  $Al_2MnH_6$ , and  $Li_2CuH_6$  show promising energetic stability and  $T_c$  of more than 50 K at ambient pressure. This study underscores promising high- $T_c$  compounds at ambient pressure with distinctive  $MH_6$  motifs.

### 1. Introduction

The idea of metallic hydrogen processing a significant high-pressure superconductivity was suggested by Abrikosov [1] and Ashcroft [2] a long time ago. However, the problem of making metallic hydrogen remains unsolved [3], and the search for corresponding superconductivity was shifted to the area of systems with partial hydrogen content, assuming that in such compounds, one can reduce the physical pressure of hydrogen metallization due to chemical pressure. In this way, the first superconducting hydride  $Th_4H_{15}$  with  $T_c \sim 8.05\text{--}8.35$  K was reported in 1970 [4]. After that, the superconductivity of the Pd-H system was discovered with a  $T_c$  of 8–9 K [5]. The Pd-(Cu, Ag, and Au)-H system was also deeply studied with  $T_c$  of 16.6, 15.6, and 13.6 K [6]. It appears that chemical pressure was not strong enough, and hydride superconductivity research in recent years has shifted to using both physical high-pressure and chemical pressure ideas with many successful discoveries, including theoretical ones. Many H-rich binary [7–12] and ternary [13–27] compounds have been predicted to be promising conventional superconductors with high  $T_c$  under high pressure, using state-of-the-art crystal structure search methods [28–32]. Among them,  $H_3S$  [33],  $LaH_{10}$  [34,35],  $CaH_6$  [36,37],  $YH_9$  [38–40],  $YH_6$  [38],

$La-Ce-H$  [41,42],  $La-Y-H$  [43],  $La-Al-H$  [44],  $La-Ba-H$  [45], and  $La-Nb-H$  [46] have been experimentally confirmed to have a  $T_c$  above 100 K under high pressures.

These remarkable discoveries represent a significant milestone, suggesting that conventional mechanisms through electron-phonon interaction can achieve superconductivity close to room temperature [47,48]. Although hydrides can trap H atoms within their host lattice to achieve superconductivity, the extremely high-pressure conditions required to stabilize the structures are still challenging. It has only been attained in a few experiments and hinders their practical applications. Therefore, the research on superconductivity in hydrides necessitates a shift toward exploring novel H-rich compounds that can be superconducting at ambient pressure.

Extensive theoretical calculations have been conducted to shed light on ambient-pressure superconducting hydrides. Vocaturo et al. predicted that  $PdCuH_2$  possesses superconducting properties with  $T_c \sim 34$  K at ambient pressure [49].  $Al_4H$  ( $Pm-3m$  space group) [50] and  $(Be_4)_2H$  (by combining  $hcp$  H and Be) [51] were also predicted to have  $T_c$  of 54 and 72–84 K, respectively. However, these two structures are both metastable with energy above convex hull ( $E_d$ ) of 136 and 202 meV/atom [52]. Using machine-learning accelerated high-throughput

\* Corresponding author.

\*\* Corresponding author.

E-mail addresses: [wsq@xmu.edu.cn](mailto:wsq@xmu.edu.cn) (S. Wu), [yangsun@xmu.edu.cn](mailto:yangsun@xmu.edu.cn) (Y. Sun).

<sup>1</sup> These authors contributed equally to this work.

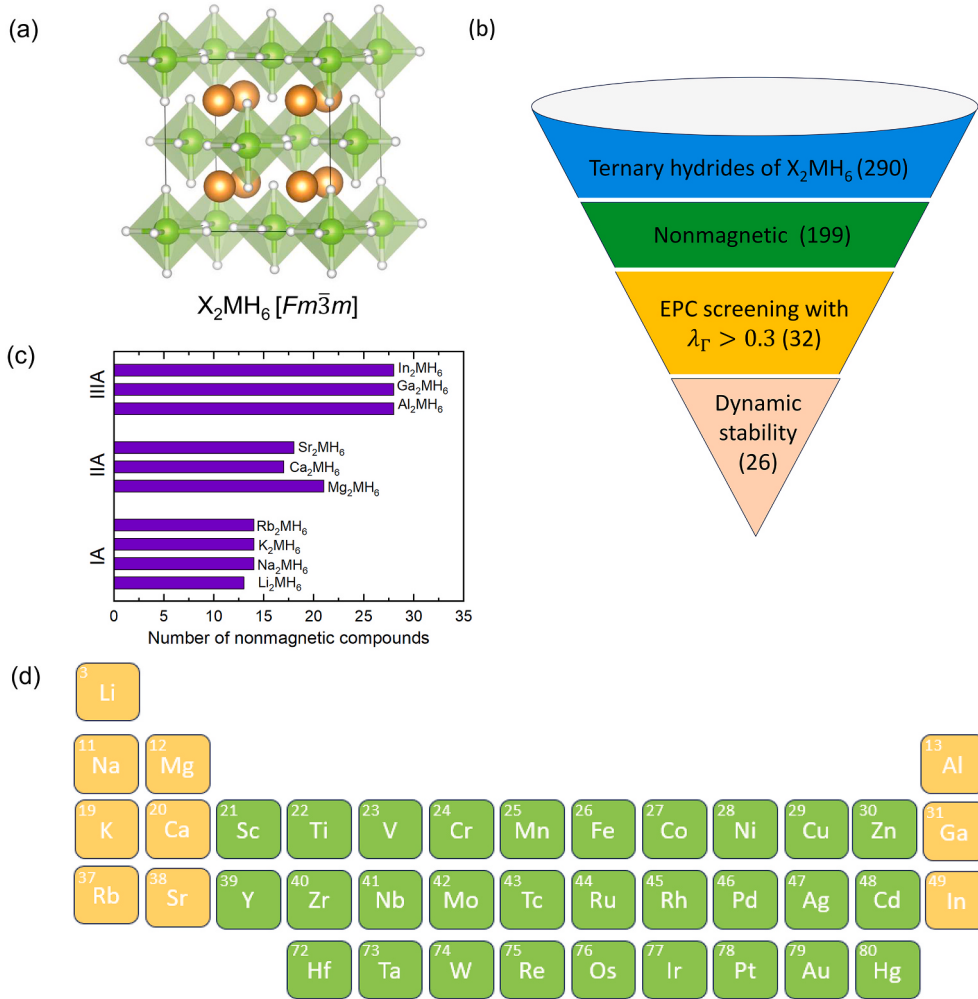


**Fig. 1.** (a) The prototype structure of  $X_2MH_6$ . The  $X$ ,  $M$ , and  $H$  atoms are colored in orange, green and white, respectively. (b) Schematic of screening workflow. (c) The number of nonmagnetic compounds of  $X_2MH_6$  with  $X$  in different groups. (d) The elements involved in the screening. Orange indicates the elements of  $X$ . Green indicates the elements of  $M$ . (For interpretation of the references to color in this figure legend, the reader is referred to the Web version of this article.)

techniques, Tiago et al. identified several hydride and hydrogen-containing materials with high- $T_c$  at ambient pressure, such as  $Li_2PdH_2$  (43 K),  $PdH$  (37 K),  $ZrH_3$  (24.9 K), and  $KCdH_3$  (23.4 K) [53]. Very recently, by employing *ab initio* random structure search (AIRSS) across the periodic table, Dolui et al. predicted cubic  $Mg_2IrH_6$  to be a superconductor at ambient pressure, with the  $T_c$  up to 160 K [54]. The  $Mg_2IrH_6$  is isostructural with the  $Mg_2FeH_6$  family [55], which was previously synthesized. Sanna et al. also investigated the superconducting properties of the  $Mg_2MH_6$  family ( $M = Rh$ ,  $Ir$ ,  $Pd$ , and  $Pt$ ) and suggested their superconducting  $T_c$  are in the range of 45–80 K [52]. The crystal structure of  $Mg_2MH_6$  is a cubic phase with an  $MH_6$  octahedron structural motif. A natural question remains whether other ternary superconducting hydrides can be stabilized in this structural framework at ambient pressure.

In this paper, we employ our recently developed fast screening method [56] to investigate the possible superconductivity in cubic  $X_2MH_6$  compounds ( $X = Li$ ,  $Na$ ,  $Mg$ ,  $Al$ ,  $K$ ,  $Ca$ ,  $Ga$ ,  $Rb$ ,  $Sr$  and  $In$ ;  $M$  is  $3d$ ,  $4d$ , and  $5d$  transition metal) at ambient pressure. The screening is based on the electron-phonon coupling strength (EPC) at the  $\Gamma$  point ( $\lambda_\Gamma$ ), which was found to be an efficient descriptor to identify conventional superconducting materials in hydrides and borides [14,56–61]. We will explore their superconducting behavior, energetic and dynamic stabilities under ambient conditions.

## 2. Computational methods

The structure optimizations were performed by using the projector-augmented wave (PAW) [62] representations with density functional theory implemented in the Vienna *ab initio* simulation package (VASP) [63,64]. The exchange and correlation energy is treated within the spin-polarized generalized gradient approximation (GGA) and parameterized by Perdew-Burke-Ernzerhof (PBE) formula [65]. A plane-wave basis was used with a kinetic energy cutoff of 520 eV. Brillouin zone integrations were approximated by using special  $k$ -point sampling of the Monkhorst-Pack scheme [66] with  $2\pi \times 0.02\text{\AA}^{-1}$ . Lattice vectors and atomic coordinates were fully relaxed until the force on each atom was less than  $0.01 \text{ eV} \cdot \text{\AA}^{-1}$ . The fast screening of EPC constant  $\lambda_\Gamma$  at the Brillouin zone center was carried out based on the frozen-phonon method [56]. Here, the  $\lambda_\Gamma$  can be defined by

$$\lambda_\Gamma = \sum_v \lambda_{\Gamma v}, \quad (1)$$

where  $\sum_v$  indicates the summation of all modes at zone-center  $\Gamma$ .  $\lambda_{\Gamma v}$  is defined by

$$\lambda_{\Gamma v} = \frac{\tilde{\omega}_{\Gamma v}^2 - \omega_{\Gamma v}^2}{4\omega_{\Gamma v}^2} \quad (2)$$

where the  $\omega_{\Gamma v}$  and  $\tilde{\omega}_{\Gamma v}$  are screened and unscreened phonon frequencies of mode  $v$  at zone-center, respectively. The zone-center phonon was computed by the PHONOPY software [67,68], with a k-point sampling grid of  $2\pi \times 0.02\text{Å}^{-1}$  spacing and a criterion of self-consistent calculation  $10^{-8}$  eV.

The full Brillouin-zone EPC calculation was performed with the Quantum ESPRESSO (QE) code [69,70] based on the density-functional perturbation theory (DFPT) [71]. The pseudopotentials (stringent norm-conserving set) from the PSEUDODOJO project [72] for PBE functional were used. The kinetic energy cutoffs were 120 Ry for wave functions and 600 Ry for potentials. Monkhorst–Pack’s sampling scheme [66] was adopted for Brillouin-zone sampling with a k-point grid of  $2\pi \times 0.02\text{ Å}^{-1}$ . The DFPT calculations were performed with the k-mesh of exactly the sampling scheme and set the q-mesh to half of the k-mesh. The convergence threshold for self-consistency was  $1 \times 10^{-14}$  Ry.

The calculations of superconducting  $T_c$  are based on the Eliashberg spectral equation  $\alpha^2 F(\omega)$  defined commonly now as

$$\alpha^2 F(\omega) = \frac{1}{2\pi N(E_f)} \sum_{qv} \frac{\gamma_{qv}}{\hbar\omega_{qv}} \delta(\omega - \omega_{qv}), \quad (3)$$

where  $N(E_f)$  is the density of states at the Fermi level,  $\omega_{qv}$  denotes the phonon frequency of the mode  $v$  with wave vector  $\mathbf{q}$ .  $\gamma_{qv}$  is the phonon linewidth defined as

$$\gamma_{qv} = \frac{2\pi\omega_{qv}}{\Omega_{BZ}} \sum_{ij} \int d^3k |g_{k,qv}^{ij}|^2 \delta(\epsilon_{q,i} - E_f) \delta(\epsilon_{k+q,j} - E_f), \quad (4)$$

where  $\epsilon_{q,i}$  and  $\epsilon_{k+q,j}$  are eigenvalues of Kohn-Sham orbitals at given bands and vectors.  $\mathbf{q}$  and  $\mathbf{k}$  are wave vectors, and  $i$  and  $j$  denote indices of energy bands.  $g_{k,qv}^{ij}$  is the EPC matrix element. The EPC constant  $\lambda$  can be determined through summation over the first Brillouin zone or integration of the spectral function in frequency space,

$$\lambda = \sum_{qv} \lambda_{qv} = 2 \int \frac{\alpha^2 F(\omega)}{\omega} d\omega, \quad (5)$$

where the EPC constant  $\lambda_{qv}$  for mode  $v$  at wave vector  $\mathbf{q}$  using Eq. (5) can be written as

$$\lambda_{qv} = \frac{\gamma_{qv}}{\pi\hbar N(E_f)\omega_{qv}^2}. \quad (6)$$

The superconducting  $T_c$  is determined with the analytical McMillan equation modified by the Allen-Dynes (A-D) equation [73,74],

$$T_c = \frac{\omega_{log}}{1.2} \exp \left[ \frac{-1.04(1+\lambda)}{\lambda(1-0.62\mu^*) - \mu^*} \right], \quad (7)$$

where  $\omega_{log}$  is the logarithmic average frequency

$$\omega_{log} = \exp \left[ \frac{2}{\lambda} \int \frac{d\omega}{\omega} \alpha^2(\omega) F(\omega) \log \omega \right] \quad (8)$$

and the effective screened Coulomb repulsion constant  $\mu^*$  was 0.1 in our calculations.

### 3. Results and discussions

#### 3.1. High throughput screening of superconductivity in $X_2MH_6$

**Fig. 1** summarizes our screening process of superconducting ternary hydrides at ambient pressure. As shown in **Fig. 1(a)**, the prototype structure  $X_2MH_6$  is a cubic phase with  $MH_6$  octahedron structural motif, which is isostructural with  $Mg_2FeH_6$  [55]. By replacing X with Li, Na, Mg, Al, K, Ca, Ga, Rb, Sr, and In, and M with 3d, 4d, and 5d transition

**Table 1**

The zone-center EPC strength ( $\lambda_{\Gamma}$ ) and energy above convex hull ( $E_d$ ) for 26 dynamically stable ternary hydrides.

Ternary hydrides	$\lambda_{\Gamma}$	$E_d$ (meV/atom)
$Mg_2RhH_6$	6.23	0
$Mg_2IrH_6$	3.27	0
$Ca_2PtH_6$	0.75	9
$Mg_2CoH_6$	0.42	29
$Al_2MnH_6$	0.96	80
$Li_2CuH_6$	0.41	80
$Ca_2PdH_6$	0.40	97
$Sr_2CuH_6$	0.31	99
$Ca_2CuH_6$	0.32	109
$Na_2CuH_6$	0.30	112
$Na_2AuH_6$	0.31	113
$Rb_2CuH_6$	0.30	113
$Al_2TeH_6$	1.67	127
$In_2TcH_6$	1.27	151
$Ga_2TcH_6$	0.70	172
$Mg_2PtH_6$	1.56	185
$In_2MnH_6$	0.32	210
$Li_2AuH_6$	0.64	217
$K_2AgH_6$	0.30	259
$Rb_2AgH_6$	0.31	266
$Na_2AgH_6$	0.31	286
$Rb_2CdH_6$	0.35	324
$Ga_2RuH_6$	0.65	327
$K_2CdH_6$	0.65	386
$Rb_2ZnH_6$	1.35	422
$Ga_2MnH_6$	1.14	778

metals (seen in **Fig. 1(d)**), we generate 290 candidates for screening. The screening criteria are shown in **Fig. 1 (b)**. The  $X_2MH_6$  compounds are all relaxed by the structural optimization at 0 GPa. After spin-polarized calculations, we remove magnetic compounds (magnetic moments are larger than  $0.3 \mu_B/\text{M}$ ) since the conventional superconductivity is mutually exclusive with magnetism. This step reduces the population of the candidate pool to 199 compounds. We find that the number of nonmagnetic compounds of  $X_2MH_6$  can be influenced by the different groups of X ions, as shown in **Fig. 1(c)**.  $X_2MH_6$  with X in the IIIA group has the highest number of nonmagnetic compounds, followed by those in the IIA and IA groups. These nonmagnetic compounds are screened by the zone-center EPC strength calculations. By setting a threshold of 0.3 ( $\lambda_{\Gamma} > 0.3$ ), 32 materials are selected for further calculations. Among them, 26 compounds are dynamically stable. To evaluate their thermodynamic stability, the energy above the convex hull ( $E_d$ ) is computed and shown in **Table 1**. The reference phases in the convex hulls are obtained from the Material Project database [75]. The  $E_d$  represents the energy of a material to decompose into a set of stable phases. A phase is stable if the  $E_d = 0$ . However, a metastable phase with small  $E_d$  can also be synthesized, given that many registered structures in the Inorganic Crystal Structure Database (ICSD) are metastable, according to a recent survey [76]. We employ the  $E_d$  less than 80 meV/atom as the criterion. This is a typical energy range to identify compounds with good experimental synthesizability [76]. After these screening, six low-energy superconductors are ultimately identified, i.e.,  $Mg_2CoH_6$ ,  $Mg_2RhH_6$ ,  $Mg_2IrH_6$ ,  $Ca_2PtH_6$ ,  $Al_2MnH_6$  and  $Li_2CuH_6$ . We then conduct full Brillouin-zone EPC and  $T_c$  calculations and identify four compounds with  $T_c$  greater than 50 K at ambient pressure, i.e.,  $Mg_2RhH_6$ ,  $Mg_2IrH_6$ ,  $Al_2MnH_6$  and  $Li_2CuH_6$ . The convex hulls of these four compounds are plotted in **Fig. S1**. The  $Mg_2RhH_6$  and  $Mg_2IrH_6$  are ground states and have a high possibility of synthesis. The  $Al_2MnH_6$  and  $Li_2CuH_6$  have  $E_d$  of 80 meV/atom and may require a suitable reaction condition to realize in experiments. *Ab initio* molecular dynamics (AIMD) simulations were conducted to examine the thermal stability as shown in **Fig. S2**. The four low-energy superconducting hydrides do not show any phase transition, which suggests they are all stable at liquid-nitrogen temperature. The superconducting behaviors of these four compounds are studied in the next section. In supporting information, the superconductivity

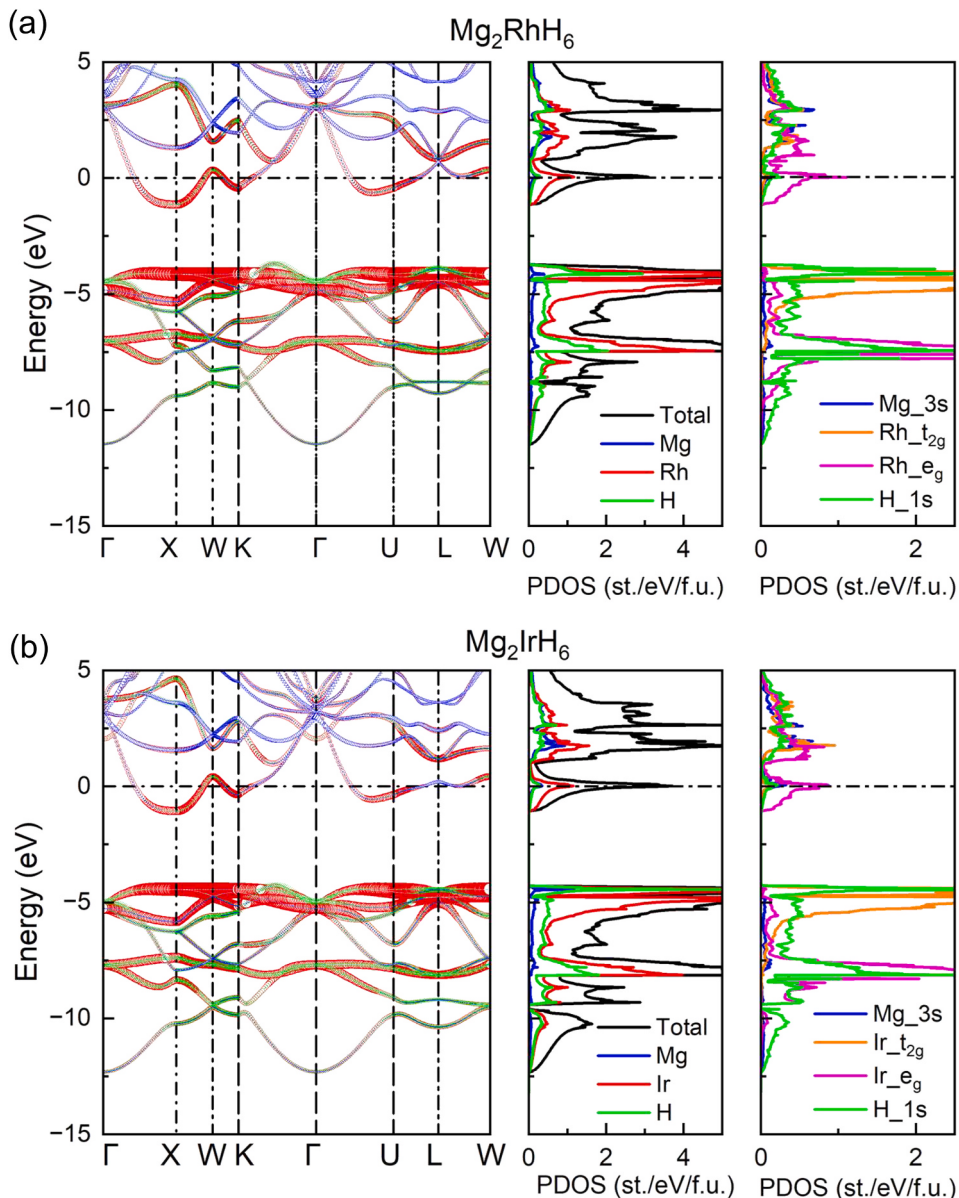


**Fig. 2.** The electronic band structure and density of states projected into atoms and orbitals for (a)  $\text{Mg}_2\text{RhH}_6$  and (b)  $\text{Mg}_2\text{IrH}_6$ .

calculations for the remaining compounds are shown in Figs. S3–S10.

### 3.2. Superconductivity of $\text{Mg}_2\text{RhH}_6$ , $\text{Mg}_2\text{IrH}_6$ , $\text{Al}_2\text{MnH}_6$ and $\text{Li}_2\text{CuH}_6$

#### A. $\text{Mg}_2\text{RhH}_6$ and $\text{Mg}_2\text{IrH}_6$

Fig. 2 shows the band structures and density of states projected into atoms and orbitals for  $\text{Mg}_2\text{RhH}_6$  and  $\text{Mg}_2\text{IrH}_6$ . One can see that both materials have nearly identical electronic structures, with a nearly isolated peak of DOS at the Fermi level ( $E_F$ ). The total DOS at  $E_F$  are 3.09 and 3.17 eV<sup>-1</sup> per f.u. for  $\text{Mg}_2\text{RhH}_6$  and  $\text{Mg}_2\text{IrH}_6$ , respectively. Near the  $E_F$ , the states are predominantly composed of transition metals  $e_g^*$  antibonding states mixed with H-1s ( $\sim 0.30$  and  $\sim 0.28$  eV<sup>-1</sup> per f.u. for  $\text{Mg}_2\text{RhH}_6$  and  $\text{Mg}_2\text{IrH}_6$ , respectively) and Mg-3s states. The corresponding charge density distribution in  $\text{MH}_6$  polyhedron for  $\text{Mg}_2\text{RhH}_6$  and  $\text{Mg}_2\text{IrH}_6$  are shown in Fig. S11. The  $e_g$  orbitals point toward nearest H neighbors, forming antibonding states, contributing to the peak of DOS at the  $E_F$ . In the valence band of these two compounds, sharp peaks are observed in the  $t_{2g}$  states to the bands along the high-symmetry path. The  $t_{2g}$  nonbonding bands of  $\text{Mg}_2\text{RhH}_6$  and  $\text{Mg}_2\text{IrH}_6$  exhibit a significant

energy gap with their  $e_g^*$  antibonding states of  $\sim 2.6$  and  $\sim 3.3$  eV, respectively. The  $e_g$  bonding bands at a lower energy level also display a sharp peak. We note that the summation of the projected DOS in the PAW sphere is smaller than the total DOS because of significant charge accumulations in the interstitial region. The interstitial contribution to the DOS at the Fermi level is significant at all energies in these systems. The electron localization functions (ELF) are calculated to understand the bonding character of  $\text{Mg}_2\text{RhH}_6$  and  $\text{Mg}_2\text{IrH}_6$  as shown in Fig. S12. Two compounds exhibit strong ELF surrounding H atoms (ELF = 1). In addition, significant charge is distributed in the interstitial regions within the  $\text{MH}_6$  octahedron, forming almost ideal electron gas (ELF  $\sim 0.5$ ) in the  $\text{MH}_6$  octahedra. Out of the  $\text{MH}_6$  octahedra, there are almost no electron distributions.

Fig. 3 displays the phonon linewidth ( $\gamma_{qv}$ )-weighted phonon spectrum, the projected phonon density of states (PHDOS), and Eliashberg spectral function  $\alpha^2F(\omega)$  for  $\text{Mg}_2\text{RhH}_6$  and  $\text{Mg}_2\text{IrH}_6$ . The phonon spectra of these two compounds are divided into three distinct regions. In the low-frequency region, the spectra are primarily dominated by transition metals and Mg atoms. The intermediate and high-frequency regions mainly arise from the vibrations of H atoms. As depicted in Fig. 3(a), for

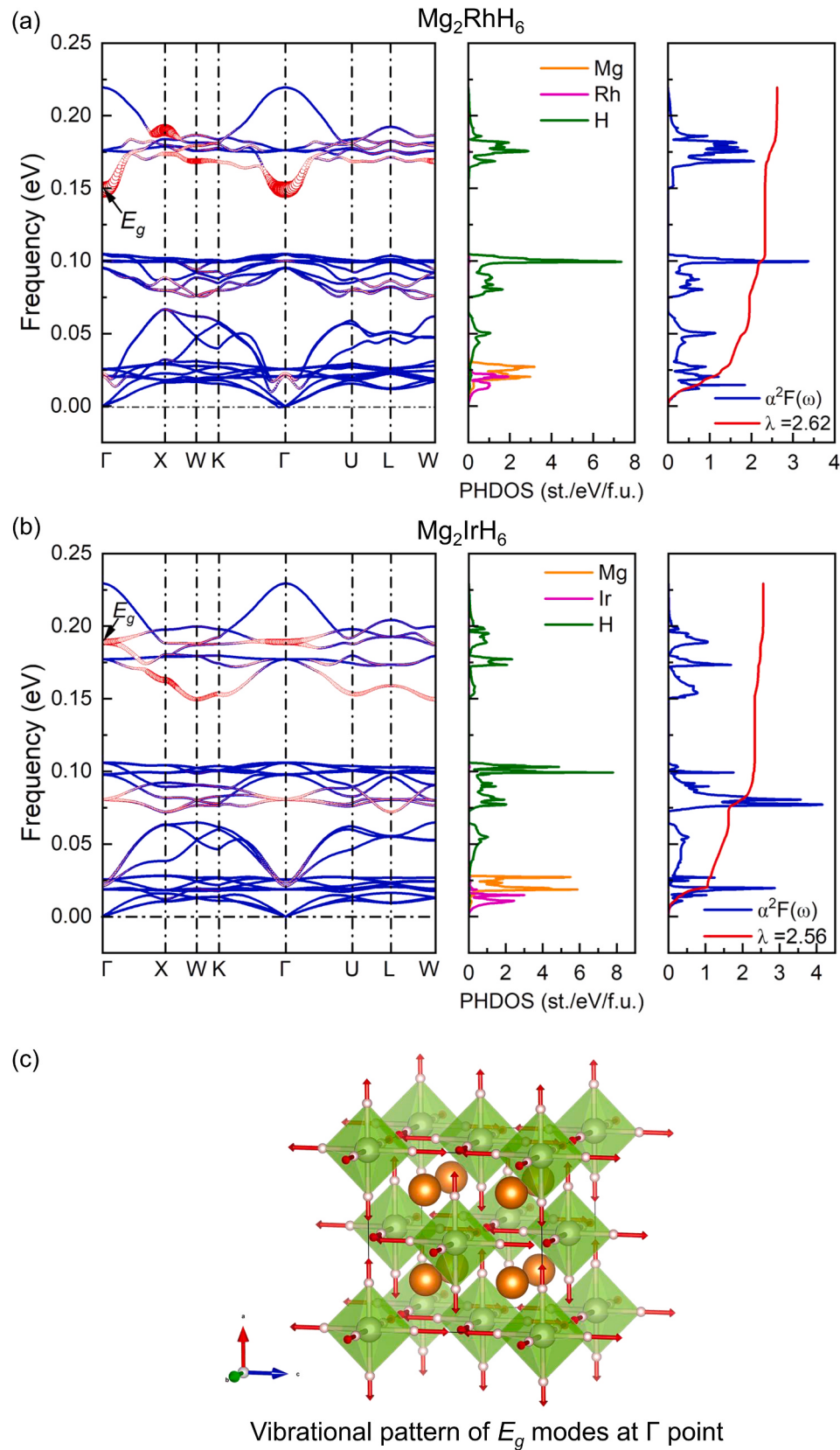


**Fig. 3.** The  $\gamma_{qv}$ -weighted (red circles) phonon spectrum, projected phonon density of states (PHDOS) and Eliashberg spectral function  $\alpha^2 F(\omega)$  for (a)  $\text{Mg}_2\text{RhH}_6$  and (b)  $\text{Mg}_2\text{IrH}_6$ . (c) The vibration pattern for double degenerate  $E_g$  modes at the  $\Gamma$  point. Red arrows denote the displacements. (For interpretation of the references to color in this figure legend, the reader is referred to the Web version of this article.)

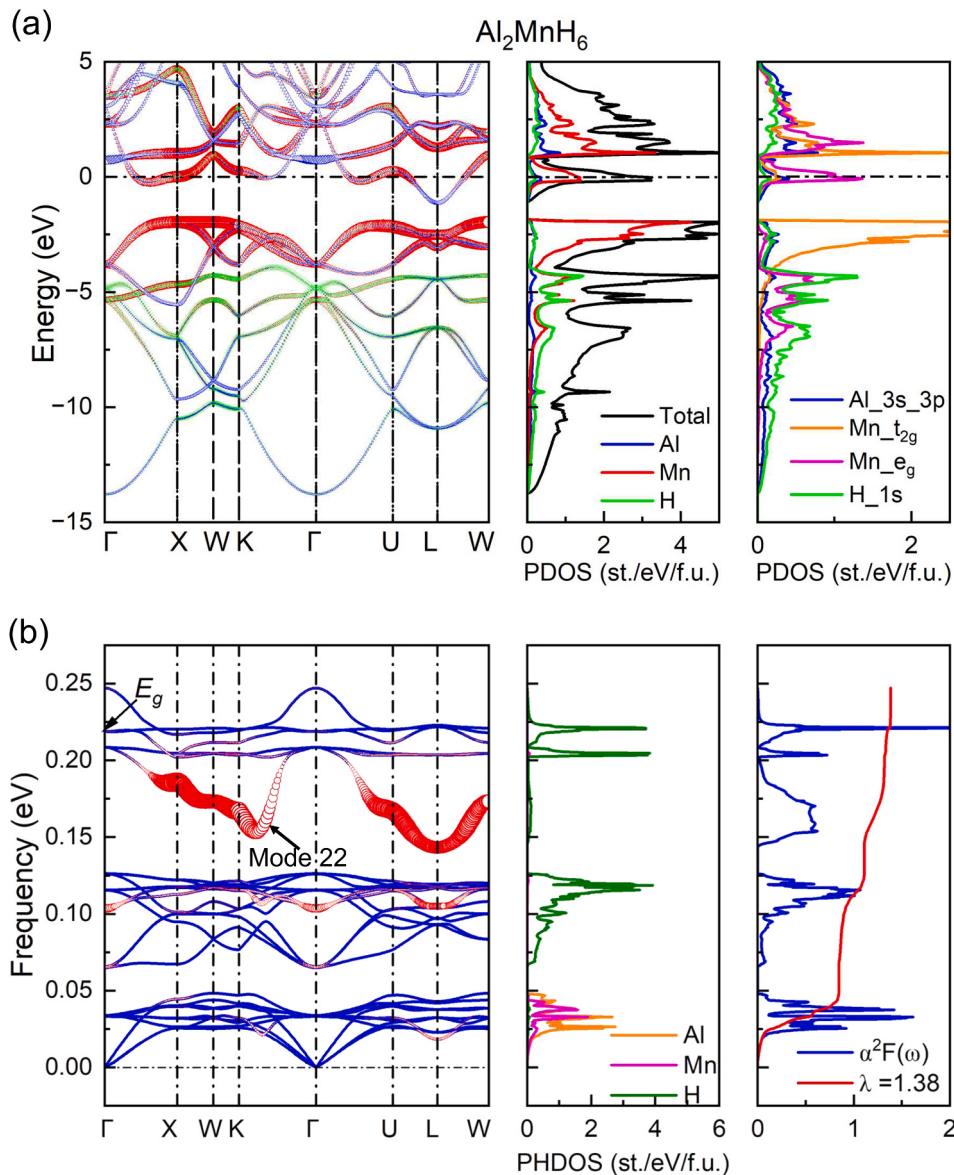


**Fig. 4.** Electronic structure and electron-phonon calculations for  $\text{Al}_2\text{MnH}_6$ . (a) Electronic band structure and density of states projected into atoms and orbital. (b) The  $\gamma_{qv}$ -weighted (red circles) phonon spectrum, projected phonon density of states (PHDOS) and Eliashberg spectral function  $\alpha^2 F(\omega)$ . (For interpretation of the references to color in this figure legend, the reader is referred to the Web version of this article.)

$\text{Mg}_2\text{RhH}_6$ , the high-frequency H modes significantly contribute to the phonon linewidth, especially the double degenerate phonon modes  $E_g$  at the  $\Gamma$  point. Their vibrational modes are shown in Fig. 3(c), which involve the breathing vibrations of H atoms in the  $\text{MH}_6$  octahedra. The intermediate-frequency region from  $\sim 0.075$  to  $\sim 0.105$  eV and low-frequency modes at  $\sim 0.021$  eV along  $\Gamma$  point corresponding to H vibrations also exhibit phonon linewidth. The integrated EPC parameter  $\lambda$  for  $\text{Mg}_2\text{RhH}_6$  is 2.62. The logarithmic average frequency ( $\omega_{\log}$ ) can be derived from the A-D equation of 352.9 K. The  $T_c$  is predicted to be 59 K. Similar to  $\text{Mg}_2\text{RhH}_6$ , the phonon linewidth in  $\text{Mg}_2\text{IrH}_6$  is primarily contributed by high and intermediate-frequency H modes, as shown in Fig. 3(b). The high-frequency phonon modes in  $\text{Mg}_2\text{IrH}_6$  show slight hardening compared to  $\text{Mg}_2\text{RhH}_6$ , where the frequency of  $E_g$  modes increases from 0.149 to 0.189 eV. The EPC constant  $\lambda$  for  $\text{Mg}_2\text{IrH}_6$  is 2.56 with a  $\omega_{\log}$  of 391.4 K. The  $T_c$  is predicted to be 65 K for  $\text{Mg}_2\text{IrH}_6$ . We note the  $T_c$  of  $\text{Mg}_2\text{IrH}_6$  is lower than the values reported in recent calculations [52,54], which employed Migdal-Eliashberg equations. We found that the  $T_c$  of  $\text{Mg}_2\text{IrH}_6$  can be increased to 98 K if the actual Allen-Dynes correction with coupling and shape factors are used.

Nevertheless, in this work, we use MAD formula to provide a lower bound of  $T_c$  for the predicted compounds.

#### B. $\text{Al}_2\text{MnH}_6$

Fig. 4 (a) presents the electronic structure of  $\text{Al}_2\text{MnH}_6$ . Analogous to  $\text{Mg}_2\text{RhH}_6$  and  $\text{Mg}_2\text{IrH}_6$ , a peak of DOS is observed at  $E_f$ , contributed by somewhat flat bands along the high-symmetry path  $(2/3\Gamma-X-1/2W$  and  $1/2\Gamma-U)$ . The total DOS is  $3.25 \text{ eV}^{-1}$  per f.u., with primary contributions from transition metal (Mn) antibonding  $e_g^*$  states mixed with H ( $0.21 \text{ eV}^{-1}$  per f.u.) and Al states. The weaker Mn  $t_{2g}$  nonbonding bands are located near 2.5 eV, exhibiting a sharp peak. The Mn  $e_g$  bonding bands are at a lower energy level, showing strong hybridization with H  $1s$  bands over a broad energy range, approximately from  $-5$  to  $-14$  eV. While Mn atoms are often magnetic in typical metallic compounds, all these systems appear nonmagnetic. It is related to the much wider electronic bandwidth of transition metal states in such hydrides (see Fig. 4). The absence of magnetic instability is favorable for the developing superconductivity. We also would like to point out that cases of

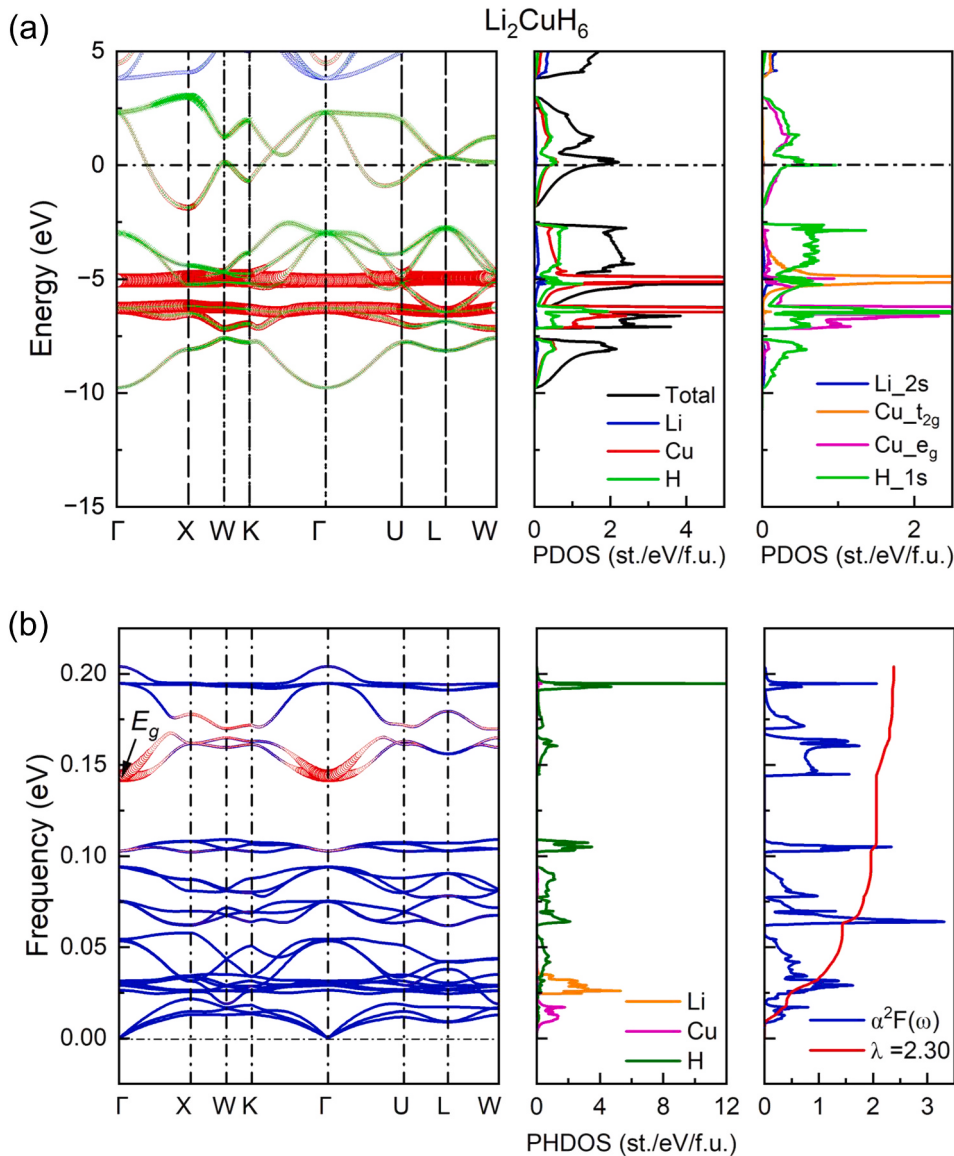


**Fig. 5.** Electronic structure and electron-phonon calculations for  $\text{Li}_2\text{CuH}_6$ . (a) Electronic band structure and density of states projected into atoms and orbital. (b) The  $\gamma_q$ -weighted (red circles) phonon spectrum, projected phonon density of states (PHDOS) and Eliashberg spectral function  $\alpha^2 F(\omega)$ . (For interpretation of the references to color in this figure legend, the reader is referred to the Web version of this article.)

electron-phonon superconductivity for Mn systems are rare.

EPC calculations for  $\text{Al}_2\text{MnH}_6$  are shown in Fig. 4(b). The phonon spectrum of  $\text{Al}_2\text{MnH}_6$  is divided into three distinct regions. The phonon modes of Al and Mn atoms are located in the low-frequency range, from 0 to  $\sim 0.048$  eV. The H modes are in two regions, from  $\sim 0.065$  to  $\sim 0.126$  eV and  $\sim 0.142$ – $\sim 0.247$  eV. Unlike  $\text{Mg}_2\text{RhH}_6$  and  $\text{Mg}_2\text{IrH}_6$ , the doubly degenerated phonon modes  $E_g$  at the  $\Gamma$  point do not exhibit a strong phonon linewidth in  $\text{Al}_2\text{MnH}_6$ . Only the high-frequency mode 22 of the H atom contributes significantly to the phonon linewidth along the Brillouin zone boundary. The H modes at  $\sim 0.102$  eV along  $\Gamma$  and L points also exhibit substantial phonon linewidth. The EPC constant  $\lambda$  for  $\text{Al}_2\text{MnH}_6$  is 1.38, lower than that of  $\text{Mg}_2\text{RhH}_6$  and  $\text{Mg}_2\text{IrH}_6$ . However, the predicted  $T_c$  of  $\text{Al}_2\text{MnH}_6$  can reach up to 66 K, due to a high logarithmic average phonon frequency  $\omega_{\log}$  ( $\sim 631.1$  K).

#### C. $\text{Li}_2\text{CuH}_6$

Fig. 5(a) displays the electronic structure of  $\text{Li}_2\text{CuH}_6$ . It also exhibits a peak of DOS at  $E_f$ , with a total DOS of  $1.51 \text{ eV}^{-1}$  per f.u., smaller than

that of  $\text{Mg}_2\text{RhH}_6$ ,  $\text{Mg}_2\text{IrH}_6$  and  $\text{Al}_2\text{MnH}_6$ . The contribution of  $\text{Cu}-e_g^*$  antibonding and H-1s states ( $\sim 0.40 \text{ eV}^{-1}$  per f.u.) is almost equal at  $E_f$ . In the valence band, the Cu  $t_{2g}$  nonbonding and  $e_g$  bonding bands exhibit sharp peaks, resulting in distinct flat bands along the entire high-symmetry path.

Fig. 5(b) presents EPC calculations for  $\text{Li}_2\text{CuH}_6$ . Like  $\text{Mg}_2\text{RhH}_6$  and  $\text{Mg}_2\text{IrH}_6$ , the doubly degenerated phonon modes  $E_g$  at the  $\Gamma$  point in  $\text{Li}_2\text{CuH}_6$  significantly contribute to the phonon linewidth, with a lower frequency of 0.143 eV. The integrated EPC parameter  $\lambda$  for  $\text{Li}_2\text{CuH}_6$  is 2.30. The  $\omega_{\log}$  derived from Eq. (8), is 500.1 K, leading to a predicted  $T_c$  of 80 K.

#### 4. Conclusions

By employing the high-throughput screening method of zone-center electron-phonon interaction, we thoroughly investigate the superconductivity of cubic ternary hydrides  $X_2\text{MH}_6$  ( $X = \text{Li}, \text{Na}, \text{Mg}, \text{Al}, \text{K}, \text{Ca}, \text{Ga}, \text{Rb}, \text{Sr}$  and  $\text{In}$ ; M is  $3d$ ,  $4d$ , and  $5d$  transition metal) at ambient pressure. We identify 26 compounds demonstrating dynamic stability with high

$\lambda_{\Gamma}$ . Among these, several have been verified to be superconductors through our EPC calculations. Notably, four compounds ( $Mg_2RhH_6$ ,  $Mg_2IrH_6$   $Al_2MnH_6$  and  $Li_2CuH_6$ ) have a  $T_c$  above 50 K and a low energy above convex hull ( $E_d < 80$  meV/atom), making them promising candidates for experimental synthesis. The  $T_c$  of  $Li_2CuH_6$  is 80 K, which is higher than the liquid-nitrogen temperature. The obtained electronic structures of these four isoelectronic compounds are similar with a generic peak of the density of states at the Fermi level. Our study indicates a significant number of candidates displaying superconductivity in cubic ternary hydrides  $X_2MH_6$  system at ambient pressure, which also demonstrates an effective strategy to explore conventional superconductors in ternary hydrides by taking into account distinctive structural motifs like  $MH_6$  octahedron. This work is expected to reignite interest in investigating the new ternary hydrides with high  $T_c$  at ambient pressure.

### CRediT authorship contribution statement

**Feng Zheng:** Writing – review & editing, Writing – original draft, Visualization, Validation, Project administration, Investigation, Funding acquisition, Formal analysis, Data curation. **Zhen Zhang:** Writing – review & editing, Writing – original draft, Visualization, Validation, Software, Methodology, Investigation, Formal analysis, Data curation. **Zepeng Wu:** Data curation, Formal analysis, Investigation, Methodology, Validation, Visualization, Writing – review & editing. **Shunqing Wu:** Writing – review & editing, Visualization, Resources, Formal analysis. **Qiubao Lin:** Writing – review & editing, Resources, Formal analysis. **Renhai Wang:** Visualization, Formal analysis. **Yimei Fang:** Investigation, Formal analysis. **Cai-Zhuang Wang:** Supervision, Resources, Formal analysis. **Vladimir Antropov:** Writing – review & editing, Validation, Supervision, Methodology, Investigation, Formal analysis. **Yang Sun:** Writing – review & editing, Visualization, Validation, Supervision, Project administration, Methodology, Investigation, Funding acquisition, Formal analysis, Conceptualization. **Kai-Ming Ho:** Writing – review & editing, Validation, Supervision, Project administration, Formal analysis, Conceptualization.

### Declaration of competing interest

The authors declare that they have no known competing financial interests or personal relationships that could have appeared to influence the work reported in this paper.

### Data availability

Data will be made available on request.

### Acknowledgments

We thank Kirill Kovnir for helpful discussions. The work at Jimei University was supported by the Natural Science Foundation of Xiamen, China (Grant No. 3502Z202372015) and the Research Foundation of Jimei University (Grant No. ZQ2023013). The work at Xiamen University was supported by the Natural Science Foundation of Xiamen, China (Grant No. 3502Z202371007) and the Fundamental Research Funds for the Central Universities (Grant No. 20720230014). Work at Guangdong University of Technology was supported by the Guangdong Basic and Applied Basic Research Foundation (Grant No. 2022A1515012174 & 2021A1515110328). V.A. and C.-Z. W. were supported by the U.S. Department of Energy, Office of Basic Energy Sciences, Division of Materials Sciences and Engineering, including the grant of computer time at the National Energy Research Supercomputing Center (NERSC) in Berkeley. Ames National Laboratory is operated for the U.S. Department of Energy by Iowa State University under Contract No. DE-AC02-07CH11358. K.-M.H. acknowledges support from National Science Foundation Award No. DMR2132666.

### Appendix A. Supplementary data

Supplementary data to this article can be found online at <https://doi.org/10.1016/j.mtphys.2024.101374>.

### References

- [1] A.A. Abrikosov, Sov. Phys. JETP 14 (1962) 408.
- [2] N.W. Ashcroft, Phys. Rev. Lett. 21 (1968) 1748.
- [3] E. Gregoryanz, C. Ji, P. Dalladay-Simpson, B. Li, R.T. Howie, H.K. Mao, Matter Radia Extremes 5 (2020): 038101.
- [4] C.B. Satterthwaite, I.L. Toepke, Phys. Rev. Lett. 25 (1970) 741.
- [5] B. Stritzker, W. Buckel, Z. Phys. A: Hadrons Nucl. 257 (1972) 1.
- [6] B. Stritzker, Z. Phys. 268 (1974) 261.
- [7] D. Duan, Y. Liu, F. Tian, D. Li, X. Huang, Z. Zhao, H. Yu, B. Liu, W. Tian, T. Cui, Sci. Rep. 4 (2014) 6968.
- [8] F. Peng, Y. Sun, C.J. Pickard, R.J. Needs, Q. Wu, Y. Ma, Phys. Rev. Lett. 119 (2017): 107001.
- [9] H. Liu, I.I. Naumov, R. Hoffmann, N.W. Ashcroft, R.J. Hemley, Proc. Natl. Acad. Sci. U. S. A. 114 (2017) 6990.
- [10] H. Wang, J.S. Tse, K. Tanaka, T. Itaya, Y.M. Ma, Proc. Natl. Acad. Sci. U. S. A. 109 (2012) 6463.
- [11] H. Xie, Y. Yao, X. Feng, D. Duan, H. Song, Z. Zhang, S. Jiang, S.A.T. Redfern, V. Z. Kresin, C.J. Pickard, et al., Phys. Rev. Lett. 125 (2020): 217001.
- [12] A.M. Shipley, M.J. Hutchison, R.J. Needs, C.J. Pickard, Phys. Rev. B 104 (2021): 054501.
- [13] B.B. Liu, W.W. Cui, J.M. Shi, L. Zhu, J. Chen, S.Y. Lin, R.M. Su, J.Y. Ma, K. Yang, M. L. Xu, et al., Phys. Rev. B 98 (2018): 174101.
- [14] Z.P. Wu, Y. Sun, A.P. Durajski, F. Zheng, V. Antropov, K.M. Ho, S.Q. Wu, Phys. Rev. Mater. 7 (2023) L101801.
- [15] L.L. Liu, F. Peng, P. Song, X.H. Liu, L.Y. Zhang, X.W. Huang, C.Y. Niu, C.Y. Liu, W. F. Zhang, Y. Jia, et al., Phys. Rev. B 107 (2023) L020504.
- [16] K. Gao, W. Cui, J. Shi, A.P. Durajski, J. Hao, S. Botti, M.A.L. Marques, Y. Li, Phys. Rev. B 109 (2024): 014501.
- [17] Z. Zhang, T. Cui, M.J. Hutchison, A.M. Shipley, H. Song, M. Du, V.Z. Kresin, D. Duan, C.J. Pickard, Y. Yao, Phys. Rev. Lett. 128 (2022): 047001.
- [18] Y. Sun, J. Lv, Y. Xie, H. Liu, Y. Ma, Phys. Rev. Lett. 123 (2019): 097001.
- [19] Wendi Zhao, Xiaoli Huang, Zihan Zhang, Su Chen, Mingyang Du, Defang Duan, Tian Cui, Natl. Sci. Rev. (2023), <https://doi.org/10.1093/nsr/nwad307>.
- [20] S. Di Cataldo, C. Heil, W. von der Linden, L. Boeri, Phys. Rev. B 104 (2021) L020511.
- [21] X.W. Liang, A. Bergara, X.D. Wei, X.X. Song, L.Y. Wang, R.X. Sun, H.Y. Liu, R. J. Hemley, L. Wang, G.Y. Gao, et al., Phys. Rev. B 104 (2021): 134501.
- [22] M. Gao, P.J. Guo, H.C. Yang, X.W. Yan, F.J. Ma, Z.Y. Lu, T. Xiang, H.Q. Lin, Phys. Rev. B 107 (2023) L180501.
- [23] X.H. Zhang, Y.P. Zhao, G.C. Yang, Wires Comput Mol Sci 12 (2022): e1582.
- [24] M.J. Jiang, Y.L. Hai, H.L. Tian, H.B. Ding, Y.J. Feng, C.L. Yang, X.J. Chen, G. H. Zhong, Phys. Rev. B 105 (2022): 104511.
- [25] S.M. Li, H.Y. Wang, W.G. Sun, C. Lu, F. Peng, Phys. Rev. B 105 (2022): 224107.
- [26] Z.Y. Wan, R.Q. Zhang, Appl. Phys. Lett. 121 (2022): 192601.
- [27] P. Song, A.P. Durajski, Z. Hou, A. Ghaffar, R. Dahule, R. Szczęśniak, K. Hongo, R. Maezono, J. Phys. Chem. C 128 (2024) 2656.
- [28] S.Q. Wu, M. Ji, C.Z. Wang, M.C. Nguyen, X. Zhao, K. Umemoto, R. M. Wentzcovitch, K.M. Ho, J. Phys.-Condens. Mat. 26 (2014): 035402.
- [29] Y. Wang, J. Lv, L. Zhu, Y. Ma, Comput. Phys. Commun. 183 (2012) 2063.
- [30] J. Wang, H. Gao, Y. Han, C. Ding, S. Pan, Y. Wang, Q. Jia, H.T. Wang, D. Xing, J. Sun, Natl. Sci. Rev. 10 (2023) nwad128.
- [31] S. Saha, S. Di Cataldo, F. Giannessi, A. Cucciari, W. von der Linden, L. Boeri, Phys. Rev. Mater. 7 (2023): 054806.
- [32] W.E. Pickett, Rev. Mod. Phys. 95 (2023): 021001.
- [33] A.P. Drozdov, M.I. Eremets, I.A. Troyan, V. Ksenofontov, S.I. Shylin, Nature 525 (2015) 73.
- [34] A.P. Drozdov, P.P. Kong, V.S. Minkov, S.P. Besedin, M.A. Kuzovnikov, S. Mozaffari, L. Balicas, F.F. Balakirev, D.E. Graf, V.B. Prakapenka, et al., Nature 569 (2019) 528.
- [35] M. Somayazulu, M. Ahart, A.K. Mishra, Z.M. Geballe, M. Baldini, Y. Meng, V. V. Struzhkin, R.J. Hemley, Phys. Rev. Lett. 122 (2019): 027001.
- [36] L. Ma, K. Wang, Y. Xie, X. Yang, Y. Wang, M. Zhou, H. Liu, X. Yu, Y. Zhao, H. Wang, et al., Phys. Rev. Lett. 128 (2022): 167001.
- [37] Z.W. Li, X. He, C.L. Zhang, X.C. Wang, S.J. Zhang, Y.T. Jia, S.M. Feng, K. Lu, J. F. Zhao, J. Zhang, et al., Nat. Commun. 13 (2022) 2863.
- [38] P. Kong, V.S. Minkov, M.A. Kuzovnikov, A.P. Drozdov, S.P. Besedin, S. Mozaffari, L. Balicas, F.F. Balakirev, V.B. Prakapenka, S. Chariton, et al., Nat. Commun. 12 (2021) 5075.
- [39] E. Snider, N. Dasenbrock-Gammon, R. McBride, X. Wang, N. Meyers, K.V. Lawler, E. Zurek, A. Salamat, R.P. Dias, Phys. Rev. Lett. 126 (2021): 117003.
- [40] Y.Y. Wang, K. Wang, Y. Sun, L. Ma, Y.C. Wang, B. Zou, G.T. Liu, M. Zhou, H. B. Wang, Chin. Phys. B 31 (2022): 106201.
- [41] J. Bi, Y. Nakamoto, P. Zhang, K. Shimizu, B. Zou, H. Liu, M. Zhou, G. Liu, H. Wang, Y. Ma, Nat. Commun. 13 (2022) 5952.
- [42] W. Chen, X. Huang, D.V. Semenok, S. Chen, D. Zhou, K. Zhang, A.R. Oganov, T. Cui, Nat. Commun. 14 (2023) 1.

- [43] D.V. Semenok, I.A. Troyan, A.G. Ivanova, A.G. Kvashnin, I.A. Kruglov, M. Hanfland, A.V. Sadakov, O.A. Sobolevskiy, K.S. Pervakov, I.S. Lyubutin, Mater. Today 48 (2021) 18.
- [44] S. Chen, Y. Qian, X. Huang, W. Chen, J. Guo, K. Zhang, J. Zhang, H. Yuan, T. Cui, Natl. Sci. Rev. 11 (2024) nwad107.
- [45] Y. Song, J. Bi, Y. Nakamoto, K. Shimizu, H. Liu, B. Zou, G. Liu, H. Wang, Y. Ma, Phys. Rev. Lett. 130 (2023) 266001.
- [46] D.V. Semenok, I.A. Troyan, A.V. Sadakov, D. Zhou, M. Galasso, A.G. Kvashnin, A. G. Ivanova, I.A. Kruglov, A.A. Bykov, K.Y. Terent'ev, et al., Adv. Mater. 34 (2022) 2204038.
- [47] J.A. Flores-Livas, L. Boeri, A. Sanna, G. Profeta, R. Arita, M. Eremets, Phys. Rep. 856 (2020) 1.
- [48] L. Boeri, G.B. Bachelet, J. Phys. Condens. Matter 31 (2019) 234002.
- [49] R. Vocaturo, C. Tresca, G. Ghiringhelli, G. Profeta, J. Appl. Phys. 131 (2022) 033903.
- [50] Y. He, J. Lu, X.Q. Wang, J.J. Shi, Phys. Rev. B 108 (2023) 054515.
- [51] Y. He, J.J. Shi, Nano Lett. 23 (2023) 8126.
- [52] Antonio Sanna, F. Tiago, T. Cerqueira, Yue-Wen Fang, Ion Errea, Alfred Ludwig, A. Miguel, L. Marques, Prediction Of Ambient Pressure Conventional Superconductivity Above 80 K In Thermodynamically Stable Hydride Compounds, 2023 arXiv:2310.06804.
- [53] T.F.T. Cerqueira, A. Sanna, M.A.L. Marques, Adv. Mater. 36 (2024) 2307085.
- [54] Kapildeb Dolui, Lewis J. Conway, Christoph Heil, Timothy A. Strobel, Rohit Prasankumar, Chris J. Pickard, Feasible Route High Temperature Ambient-Pressure Hydride Superconductivity, 2023 arXiv:2310.07562.
- [55] S.S.S. Raman, D.J. Davidson, J.L. Bobet, O.N. Srivastava, J. Alloys Compd. 333 (2002) 282.
- [56] Y. Sun, F. Zhang, C.-Z. Wang, K.-M. Ho, I.I. Mazin, V. Antropov, Phys. Rev. Mater. 6 (2022) 074801.
- [57] F. Zheng, Y. Sun, R. Wang, Y. Fang, F. Zhang, S. Wu, C.-Z. Wang, V. Antropov, K.-M. Ho, Phys. Rev. B 107 (2023) 014508.
- [58] F. Zheng, Y. Sun, R.H. Wang, Y.M. Fang, F. Zhang, S.Q. Wu, Q.B. Lin, C.Z. Wang, V. Antropov, K.M. Ho, Phys. Chem. Chem. Phys. 25 (2023) 32594.
- [59] Y. Sun, Z. Zhang, A.P. Porter, K. Kovnir, K.M. Ho, V. Antropov, npj Comput. Mater. 9 (2023) 204.
- [60] R. Wang, Y. Sun, F. Zhang, F. Zheng, Y. Fang, S. Wu, H. Dong, C.Z. Wang, V. Antropov, K.M. Ho, Inorg. Chem. 61 (2022) 18154.
- [61] S. Chen, Z. Wu, Z. Zhang, S. Wu, K.-M. Ho, V. Antropov, Y. Sun, High-Throughput Screening For Boride Superconductors, 2024 arXiv:2401.13211.
- [62] G. Kresse, D. Joubert, Phys. Rev. B 59 (1999) 1758.
- [63] G. Kresse, J. Furthmuller, Phys. Rev. B 54 (1996) 11169.
- [64] G. Kresse, J. Furthmuller, Comput. Mater. Sci. 6 (1996) 15.
- [65] J.P. Perdew, K. Burke, M. Ernzerhof, Phys. Rev. Lett. 77 (1996) 3865.
- [66] H.J. Monkhorst, J.D. Pack, Phys. Rev. B 13 (1976) 5188.
- [67] A. Togo, F. Oba, I. Tanaka, Phys. Rev. B 78 (2008) 134106.
- [68] A. Togo, I. Tanaka, Scripta Mater. 108 (2015) 1.
- [69] P. Giannozzi, S. Baroni, N. Bonini, M. Calandra, R. Car, C. Cavazzoni, D. Ceresoli, G.L. Chiarotti, M. Cococcioni, I. Dabo, et al., J Phys-Condens Mat 21 (2009) 395502.
- [70] P. Giannozzi, O. Andreussi, T. Brumme, O. Bunau, M.B. Nardelli, M. Calandra, R. Car, C. Cavazzoni, D. Ceresoli, M. Cococcioni, et al., J Phys-Condens Mat 29 (2017) 465901.
- [71] S. Baroni, S. de Gironcoli, A. Dal Corso, P. Giannozzi, Rev. Mod. Phys. 73 (2001) 515.
- [72] M.J. van Setten, M. Giantomassi, E. Bousquet, M.J. Verstraete, D.R. Hamann, X. Gonze, G.M. Rignanese, Comput. Phys. Commun. 226 (2018) 39.
- [73] P.B. Allen, R.C. Dynes, Phys. Rev. B 12 (1975) 905.
- [74] P.B. Allen, Phys. Rev. B 6 (1972) 2577.
- [75] A. Jain, S.P. Ong, G. Hautier, W. Chen, W.D. Richards, S. Dacek, S. Cholia, D. Gunter, D. Skinner, G. Ceder, et al., Apl. Mater. 1 (2013) 011002.
- [76] W.H. Sun, S.T. Dacek, S.P. Ong, G. Hautier, A. Jain, W.D. Richards, A.C. Gamst, K. A. Persson, G. Ceder, Sci. Adv. 2 (2016) e1600225.